Journal of Alloys and Compounds 505 (2010) 86–90

Contents lists available at ScienceDirect

Journal of Alloys and Compounds

journal homepage: www.elsevier.com/locate/jallcom

Microstructural characterization by TEM techniques of mechanically alloyed FeNbGe powders

J.J. Ipus[a,1], J.S. Blázquez[a], A. Conde[a,*], S. Lozano-Pérez[b]

[a] Dpto. Física de la Materia Condensada, ICMSE-CSIC, Universidad de Sevilla, P.O. Box 1065, 41080 Sevilla, Spain
[b] Department of Materials, University of Oxford, Parks Road, Oxford OX1 3PH, UK

ARTICLE INFO

Article history:
Received 28 April 2010
Received in revised form 1 June 2010
Accepted 10 June 2010
Available online 18 June 2010

Keywords:
Transmission electron microscopy
Mechanical alloying
Nanocrystalline alloys

ABSTRACT

Mechanically alloyed $Fe_{75}Nb_5Ge_{20}$ alloys have been studied using different TEM techniques. For short milling times the microstructure of the system consists of an inhomogeneous mixture of the starting crystalline phases: small bcc Fe nanocrystallites, filament-like bcc Nb and spherical fcc Ge. After long milling times, the microstructure consists of a single bcc supersaturated solid solution Fe(Nb,Ge) phase.

1. Introduction

Mechanical alloying has become a very versatile technique to directly produce metastable systems, such as nanocrystalline, amorphous, supersaturated solid solutions, etc. [1]. Generally, mechanical alloying starts from a mixture of elemental powders or alloys, which progressively leads to the formation of an amorphous and/or a nanocrystalline supersaturated solid solution. Mechanical alloying is especially suitable to produce supersaturated solid solutions extending the solubility of some immiscible elements beyond the compositional range found in equilibrium conditions [1,2].

Commonly the global microstructural characterization of powder samples is performed using techniques such as X-ray diffraction (XRD), which provides a general view of the sample, characterizing the phase evolution, average values of microstructural parameters (grain size, microstrain) and compositional information derived from the evolution of lattice parameter [1,3–5]. On the other hand, image and analytical techniques using transmission electron microscopy (TEM) provides information about the local microstructure and composition distribution. This information is far beyond that obtained from XRD results, even in the detection of minority phases (not only due to small volume fractions but also to low scattering power as in the case of the detection of boron inclusions in FeNbB mechanically alloyed powders [6]). However, these kinds of studies are not extensively performed in powder samples [3,6,7] because of the difficulties associated with the TEM sample preparation.

In this study selected samples of $Fe_{75}Nb_5Ge_{20}$ alloy prepared by mechanical alloying were studied by different TEM imaging, diffraction and microanalysis techniques in order to obtain complementary information of the microstructure evolution to that previously studied by XRD and Mössbauer spectrometry [8].

In this work, two samples milled at 250 r.p.m. were chosen: after 10 h and after 150 h. SEM results show that, for short milling times with $t = 10$ h, the powder particle size reaches a minimum value of ~5 μm and the composition of powder particles is close to the nominal one for milling times larger than 10 h, with a dispersion in the Ge/(Fe + Ge) concentration ratio of ~4% for these milling times. XRD results (Fig. 1) show that, for short milling times, the diffraction maxima corresponding to the starting phases are present, along with some extra peaks ascribed to an intermetallic compound previously detected by XRD [8]. However, its identification is difficult with only one single peak. XRD results on the sample milled for 150 h only shows the formation of a single supersaturated bcc Fe(Nb,Ge) solid solution with a lattice parameter larger than that corresponding to pure α-Fe phase and a minimum crystal size ~5 nm [8].

2. Experimental

Different transmission electron microscopy techniques were used in this work: bright field (BF), dark field (DF) and high resolution (HREM) imaging, plus selected area diffraction (SAD) and convergent beam electron diffraction (CBED). Moreover, two analytical techniques were used: energy dispersive X-ray spectroscopy (EDX) and energy filtered transmission electron microscopy (EFTEM). Experiments were

* Corresponding author. Tel.: +34 95 455 28 85; fax: +34 95 461 20 97.
E-mail address: conde@us.es (A. Conde).
[1] Present address: Department of Materials Science and Engineering, Carnegie Mellon University, Pittsburgh, PA 15213, USA.

0925-8388/$ – see front matter © 2010 Elsevier B.V. All rights reserved.
doi:10.1016/j.jallcom.2010.06.034

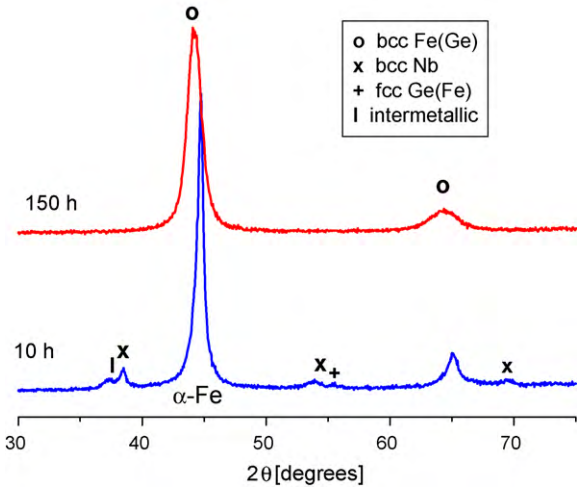

Fig. 1. XRD patterns of the two studied samples.

done using different microscopes: a Philips CM200 operated at 200 kV and a JEOL JEM3000F operated at 297 kV.

The preparation of TEM specimens was performed using a focus ion beam (FIB) FEI 200, using the in situ lift out procedure [9]. This method of preparation of the TEM samples is shown in Fig. 2 for a powder particle formed by the aggregation of several smaller ones. The main steps followed are:

A protective Pt layer is deposited on the selected powder particle to avoid damage on this area during cutting and thinning processes (Fig. 2a and b).
A slice of approximately 15 μm × 15 μm × 2 μm is cut from the powder particle (Fig. 2c and d) and later, using Pt, it is welded onto a Cu grid with the help of an in situ micromanipulator (Fig. 2e and f).
Finally, the TEM sample is thinned to electron transparency (Fig. 2g and h).

3. Results and discussion

Fig. 2h shows a global view of the sample prepared by the lift out technique. The coupling between the powder particles that form the agglomerate can be easily observed. In Fig. 3a, a BF TEM image of a closer view of the powder particle at $t = 10$ h is shown. The observed microstructure consists of a majority of small crystals with a size of ~10 nm (see Fig. 3c, a magnified view of the right region in Fig. 3a), which is in rough agreement with the XRD patterns [8], long shaped crystals (Nb rich as it will be shown later by EDX maps), as well as regular shaped crystals with a size about 100 nm (Ge-rich as it will be shown later by EDX maps). The selected area diffraction pattern (Fig. 3b) shows the non-homogeneity of the alloy with spots that can be identified as the three initial phases (bcc Fe, fcc Ge and bcc Nb).

Fig. 4 shows the EDX compositional analysis of this sample, revealing a non-homogeneous mixing of the initial elements. In this analysis the individual compositional maps for Fe, Ge and Nb and a red–green–blue RGB map (Fe, Ge and Nb, respectively) are shown. Fe rich zones can be observed, although this element is spread over the whole region studied. A similar behavior is observed in the Ge map, where a good mixing with Fe can be seen (considering the size of the crystallites of this phase) in agreement with the solid solution formed in Fe–Ge system [10]. However, large Ge-rich crystals ~100 nm are clearly identified in this map. In the case of Nb, the compositional map shows a pour mixing of this element with the Fe–Ge matrix according to its low solubility [11] and almost pure Nb crystals are found, as detected by XRD experiments [8]. Moreover, it is observed that these Nb crystals are filament-like in shape, as expected for a ductile material [1].

In order to confirm the phase distribution previously described for the sample at this milling time, convergent beam electron diffraction patterns were acquired from several crystals. All these patterns could be indexed using bcc Fe, fcc Ge or bcc Nb phases and an example for each phase is shown in Fig. 5, where the theoretical electron patterns were built using CaRine software [12]. After these results, evidence of the intermetallic compound reported for these milling times in a previous work [8] was not found. However, this cannot be taken as an evidence of its absence. This phase could be distributed in very tiny phases at the boundaries of other crystals. The presence of unindexed spots in the SAD patterns suggests the existence of other phase(s) different than those of the starting mixture but, unfortunately, does not supply enough information for a reliable phase identification.

Fig. 6 shows the microstructure of the sample milled for ~150 h as well as a SAD pattern showing the diffraction rings corresponding to the bcc Fe(Ge,Nb) solid solution. A more detailed view is shown in Fig. 7a, where regular shaped nanocrystals with an aver-

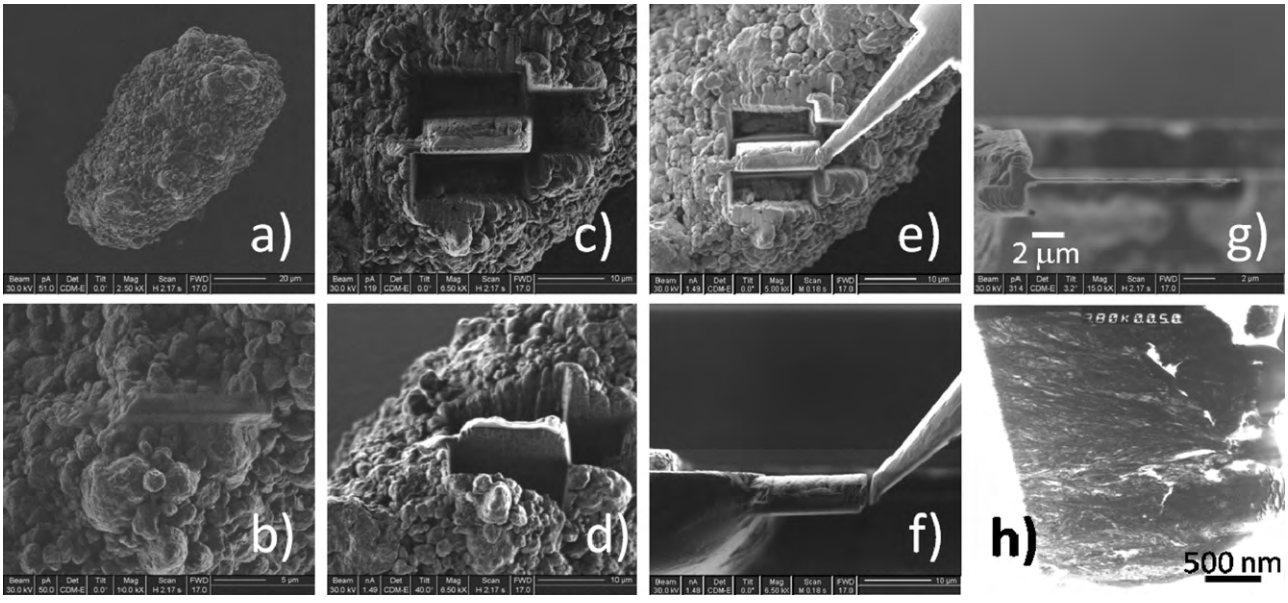

Fig. 2. TEM sample preparation procedure using FIB. FIB secondary electron images: (a) selected powder particle, (b) Pt layer deposited, (c) and (d) cutting of the sample, (e) sample welded to the micromanipulator, (f) sample welded to the TEM sample holder and cut from the micromanipulator and (g) sample thinned. (h) BF TEM image showing an overview of the sample after $t = 10$ h milling.

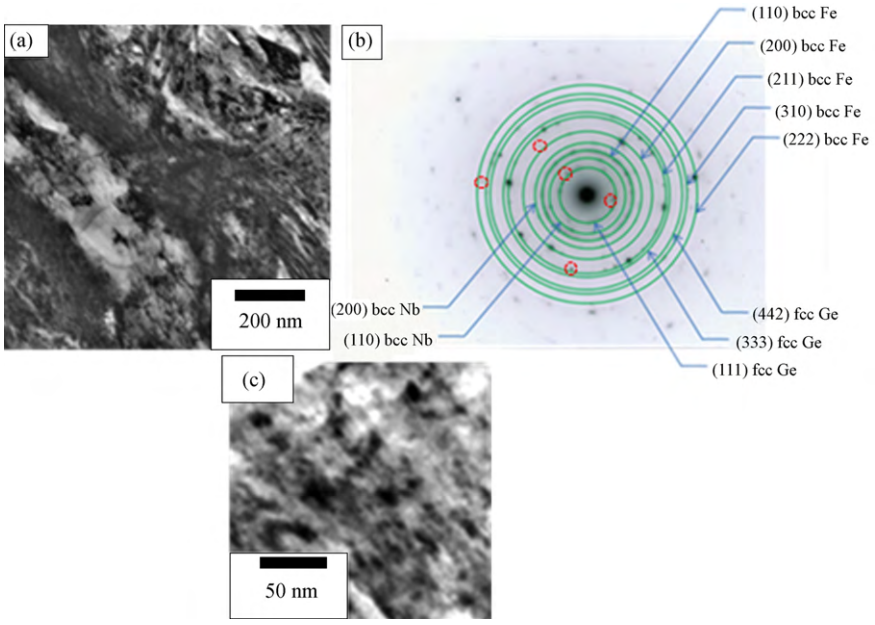

Fig. 3. (a) BF TEM image, (b) SAED pattern of the sample after $t = 10$ h milling and (c) magnified view of (a) showing α-Fe(Ge) nanocrystals The different diffraction rings corresponding to the three initial phases are indicated and some examples of unindexed spots are marked.

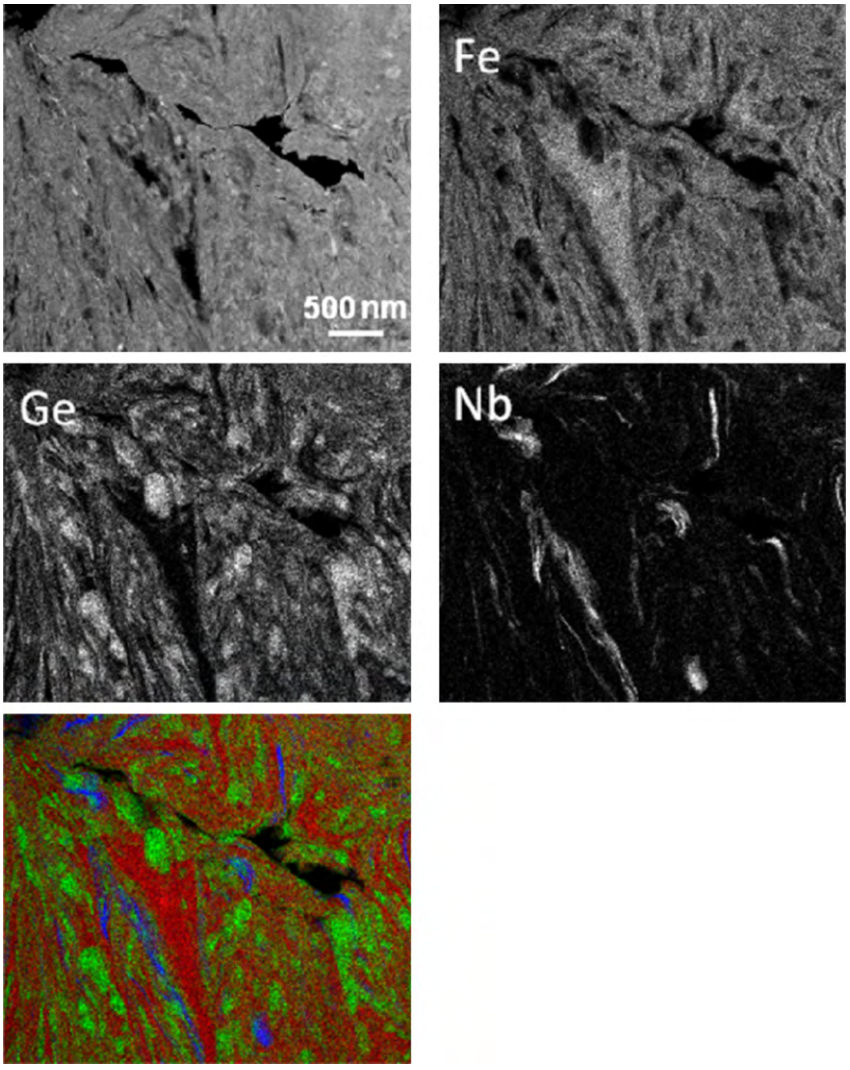

Fig. 4. High angle annular dark field (HAADF) image and EDX maps from the sample after $t = 10$ h milling. Red, green and blue correspond to Fe, Ge and Nb, respectively, in the RGB colored map. (For interpretation of the references to color in this figure legend, the reader is referred to the web version of the article.)

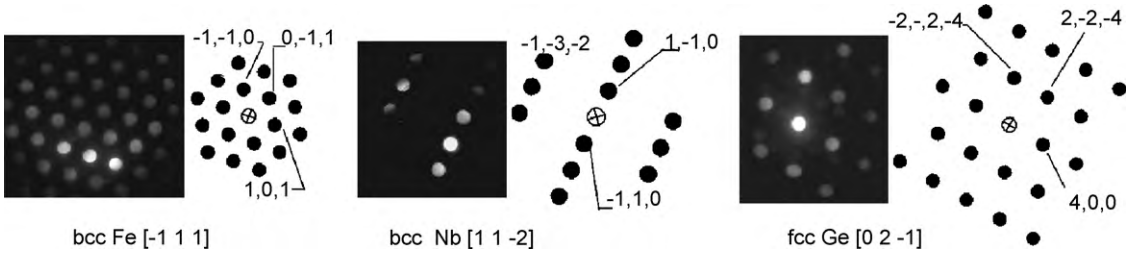

Fig. 5. CBED patterns of the sample after $t = 10$ h milling, indexed as pure bcc Fe, bcc Nb and fcc Ge.

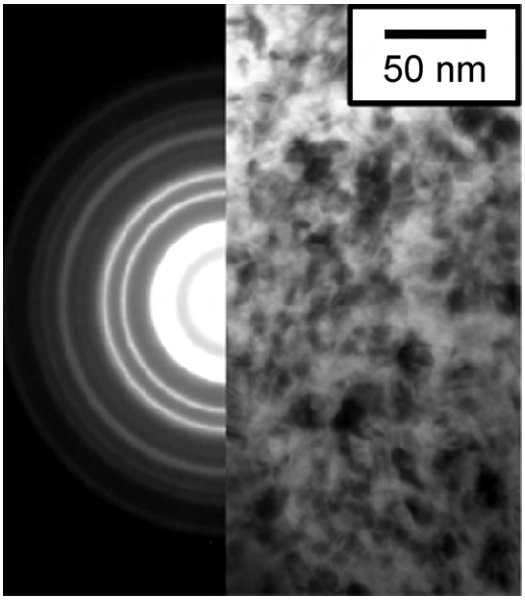

Fig. 6. SAD pattern and BF TEM image of sample after $t = 150$ h milling.

age size ~8 nm can be observed, which is in agreement with XRD experiments [8]. Filament-like Nb rich crystals do not appear for these milling times as neither do the Ge-rich inclusions, unlike boron inclusions found after milling Fe–Nb–B alloys [6]. HREM images acquired from the nanocrystalline matrix of this sample (an example is shown in Fig. 7b) can be used to measure interplanar distances, e.g.: $d_{h1,k1,l1} \approx 2.22 \pm 0.10$ Å, $d_{h2,k2,l2} \approx 1.93 \pm 0.10$ Å and $d_{h3,k3,l3} \approx 1.19 \pm 0.10$ Å, which for a cubic cell must meet:

$$\left(\frac{d_{h1,k1,l1}}{d_{h2,k2,l2}}\right)^2 = \frac{h_2^2 + k_2^2 + l_2^2}{h_1^2 + k_1^2 + l_1^2},$$

where h_i, k_i, l_i are the Miller index. The plane families of a bcc phase type satisfying the previous criteria for: $\{h_1,k_1,l_1\} = \{1,1,0\}$, $\{h_2,k_2,l_2\} = \{1,1,1\}$ and $\{h_3,k_3,l_3\} = \{2,1,1\}$ which would imply that $a \approx 3.1 \pm 0.2$ Å, in rough agreement with the bcc Fe(Ge,Nb) phase detected by XRD. The observed difference is not surprising since only small portions of the sample were used for the measurements and uncertainty in the thickness of the areas chosen, can make interpretation difficult. In order to achieve full confidence in the HREM measurements, focal series together with image simulation should have been used, but it was out of the scope of this work.

The absence of long shaped crystals for these milling times is associated with the dissolution of Nb in the microstructure developed by the nanocrystals. Fig. 8 shows EFTEM elemental maps from the Fe $L_{2,3}$ and Ge $M_{4,5}$ edges, corresponding to the zone presented in Fig. 7a. Unlike that found for Fe and B in the ternary alloy Fe–Nb–B [6], for long milling times, a good mixing of Fe and Ge was observed, as shown in Fig. 8. EFTEM images did not reveal the presence of Ge-rich zones. The absence of Ge-rich zones suggests the complete incorporation of Ge into the Fe nanocrystals and/or the boundary region as previously reported [8]. This observation could be explained by the higher solubility of Ge in α-Fe than that of B in Fe–Nb–B alloy and/or by the lower melting temperature of Ge respect to B, which allows an easier mixing between the elements, as some theoretical studies predict high local temperature in the collision events during ball milling process [1,13,14].

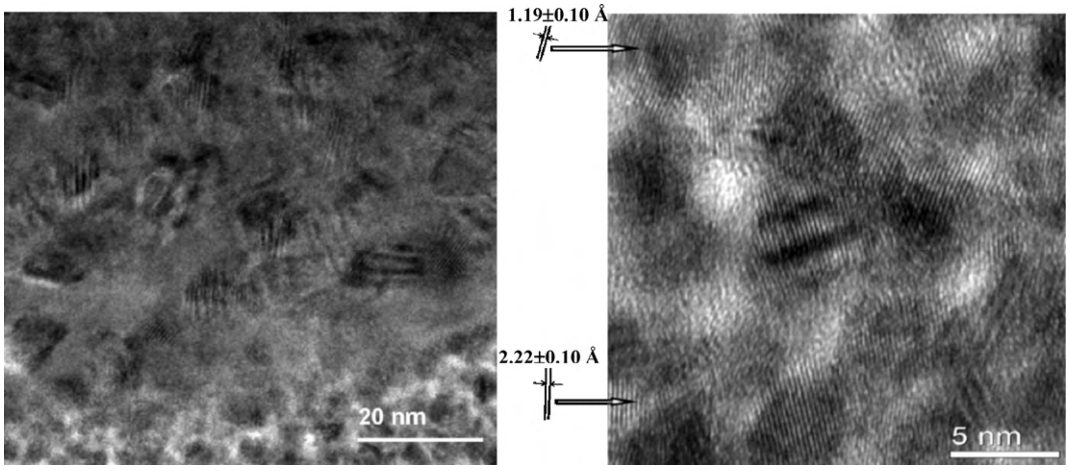

Fig. 7. (Left) BF TEM and (right) HREM images of sample after $t = 150$ h milling.

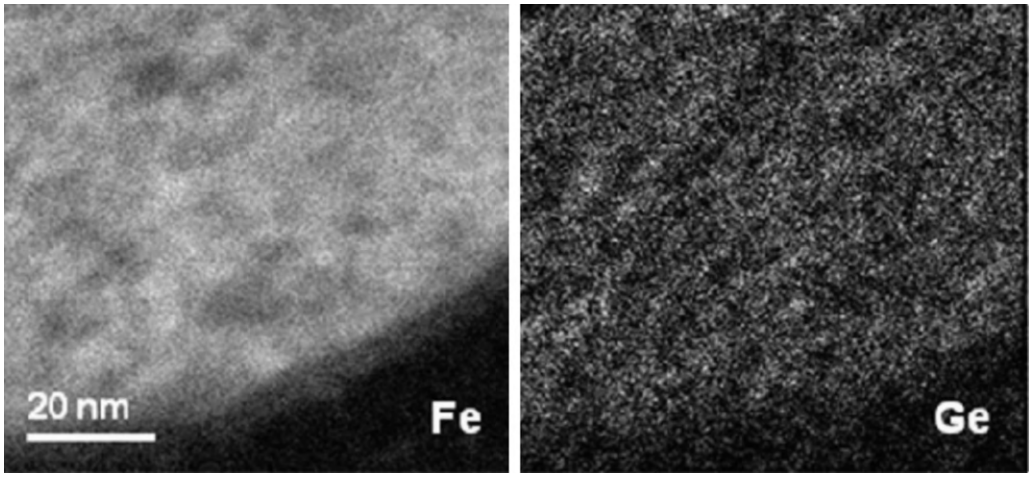

Fig. 8. EFTEM images acquired at the characteristics energies of Fe and Ge of samples after t = 150 h milling.

4. Conclusions

Microstructural and compositional partitioning has been studied on two selected samples of $Fe_{75}Nb_5Ge_{20}$ (at short milling time and long milling time, respectively) using a combination of different diffraction, imaging and analytical TEM techniques.

At short milling time, when the inhomogeneity of the sample is observed from conventional XRD, mixing of bcc Fe(Ge), almost pure bcc Nb and fcc Ge(Fe) phases can be detected. Regular shaped Fe rich (see Fig. 3c) and Ge-rich nanocrystals (see EDX maps in Fig. 4), the latter being 10 times larger, were observed, whereas the Nb crystals showed an elongated shape. As the milling time progresses, Nb and Ge crystals disappear due to the incorporation of these elements into Fe matrix to form a supersaturated solid solution bcc Fe(Nb,Ge) type phase with a homogeneous microstructure and without the presence of any inclusions.

Acknowledgements

This work was supported by the Ministry of Science and Innovation (MICINN) and EU FEDER (project. No. MAT2007-65227) and the PAI of the Regional Government of Andalucía (project. No. P06-FQM-01823). TEM investigations were supported by the IP3 project of the 6th Framework Programme of the European Commission: ESTEEM Contract number 026019. J.J.I. acknowledges a fellowship from the Spanish Ministry of Education and Science and a Postdoctoral Research Associate position from Carnegie Mellon University.

References

[1] C. Suryanarayana, Prog. Mater. Sci. 46 (2001) 1–184.
[2] Y.A. Skakov, Met. Sci. Heat Treatment 47 (2005) 296–304.
[3] J.Y. Yang, T.J. Zhang, K. Cui, X.G. Li, J. Zhang, J. Alloys Compd. 242 (1996) 153–156.
[4] J.J. Suñol, A. Gonzalez, J. Saurina, Ll. Escoda, P. Bruna, Mater. Sci. Eng. A 375–377 (2004) 874–880.
[5] A. Grabias, M. Kopcewicz, D. Oleszak, J. Alloys Compd. 339 (2002) 221–229.
[6] J.J. Ipus, J.S. Blázquez, S. Lozano-Pérez, A. Conde, Philos. Mag. 89 (2009) 1415–1423.
[7] J. Han, S. Lui, X. Zang, H. Du, C. Wang, Y. Yang, M. Yue, X. Liu, J. Appl. Phys. 101 (09) (2007) K502.
[8] J.S. Blázquez, J.J. Ipus, M. Millán, V. Franco, A. Conde, D. Oleszak, T. Kulik, J. Alloys Compd. 469 (2009) 169–178.
[9] S. Lozano-Perez, Micron 39 (2008) 320–328.
[10] A.F. Cabrera, F.H. Sánchez, Phys. Rev. B 65 (2002) 094202.
[11] A. Blachowski, K. Ruebenbauer, J. Zukrowski, Phys. Stat. Sol. (b) 15 (2005) 3201–3208.
[12] C. Boudais, D. Monceau, CaRine Crystallography 3.1, 1989–1998.
[13] J. Eckert, L. Schultz, E. Hellstern, K. Urban, J. Appl. Phys. 64 (1986) 3224–3228.
[14] M. Abdellaoui, E. Gaffet, J. Alloys Compd. 209 (1994) 351–361.